CHEMISTRY OF MATERIALS
Article

Chem. Mater. **2011,** *23,* 75–84 75
DOI:10.1021/cm102255j

Nucleation and Growth of Magnetic Ni−Co (Core−Shell) Nanoparticles in a One-Pot Reaction under Microwave Irradiation

Tomohisa Yamauchi,[†] Yasunori Tsukahara,*[,†] Katsuhiro Yamada,[‡] Takao Sakata,[§] and Yuji Wada*[,¶]

[†]*Graduate School of Engineering, Osaka University, 2-1 Yamada-oka Suita, 565-0871, Japan,* [‡]*Nippon Steel Chemical Co., Ltd., 46-80, Nakabaru Sakinohama, Tobata-Ku, Kitakyushu, Fukuoka 804-8503, Japan,* [§]*Research Center for Ultra-High Voltage Electron Microscopy, Osaka University, 7-1 Mihogaoka, Ibaraki, Osaka 567-0047, Japan, and* [¶]*Department of Applied Chemistry, Graduate School of Science and Engineering, Tokyo Institute of Technology, 2-12-12 Ookayama, Meguro, Tokyo 152-8552, Japan*

Received August 9, 2010. Revised Manuscript Received November 22, 2010

We have successfully prepared face-centered cubic (fcc) Ni−Co (core−shell) nanoparticles using both nickel(II) acetate and cobalt(II) formate complexes with oleylamine in a one-pot reaction under microwave irradiation. Observation using a high-angle annular dark-field scanning transmission electron microscope (HAADF-STEM) technique has shown that the nanostructure was composed of a Co-rich shell and a Ni-rich core. $Ni_{50}Co_{50}$ nanoparticles with an average particle size of 71.0 nm were composed of a Ni core with a diameter of ca. 46.9 nm, a ca. 10.0 nm-thick Co shell, and a ca. 4.0 nm-thick interlayer of mixed Ni−Co alloy in between. Co shells were overgrown on the Ni core. The crystalline shapes of the Ni−Co nanoparticles were easily controlled using different nickel precursors (acetate or formate complexes) as starting materials. The crystalline shape of the Ni core played a key role in determining the final shape of a Ni−Co (core−shell) nanocrystal. A formation mechanism for Ni−Co (core−shell) nanoparticles was proposed on the basis of the results of several synthetic routes. First, Ni core nanoparticles were produced at around 498 K through the redox reaction between oleylamine and Ni^{2+} in a mixture of nickel(II) acetate and cobalt(II) formate complexes with oleylamine. Then, Co^{2+} on the surface of the Ni core was easily reduced at 498 K, because Ni nanoparticles could act as a catalyst for the redox reaction between oleylamine and Co^{2+}.

1. Introduction

The synthesis of bimetallic core−shell and alloy nanoparticles[1] is significant due to their novel physical properties, which are superior to those of monometallic nanoparticles.[2] A variety of physical properties of several metal compounds with core−shell structures have been reported in relation to the luminescence of II−VI semiconductors (CdSe-CdS/ZnS core-multi shells)[3] and in catalyses for the preferential oxidation of carbon monoxide in the hydrogen or hydrolytic dehydrogenation of ammonia borane using Ru−Pt or Au−Co core−shell nanoparticles, respectively.[4] Several researchers have reported the shape-controlled syntheses and growth mechanisms of noble metal core−shell nanoparticles in hexagonal and triangular shapes.[5] Recently, inexpensive first-row, transition-metal, core−shell nanoparticles with ferromagnetic properties, such as Fe, Co, and Ni, have attracted attention due to alternative resources of noble metals[6] and novel physical properties such as superparamagnetism,[7] giant magnetoresistance,[8] or mesoscopic transport effects in magnetic tunnel junctions.[9] Metal−metal oxide (core−shell) nanoparticles such as Fe^0−Fe_xO_y, Co^0−CoO, and Ni^0−NiO can be easily prepared

*To whom correspondence should be addressed. Tel: +81-6-6878-2538 (Y.T.). Fax: +81-6-6878-2538 (Y.T). E-mail: ytsuka@jrl.eng.osaka-u.ac.jp (Y.T.); yuji-w@apc.titech.ac.jp (Y.W.).

(1) Generally speaking, three main types of mixing patterns for bimetallic alloy nanoparticles can be identified such as mixed alloy, subcluster segregated alloy, and core−shell segregated alloy.[1a] In the case of the mixed alloy, each metal is randomly dispersed without any order through the entire particle as a solid solution. The core−shell segregated alloy consists of a shell of either metal surrounding a core of another. In this paper, the mixed alloy is described as the alloy for short. (a) Ferrando, R.; Jellinek, J.; Johnston, R. L. *Chem. Rev.* **2008**, *108*, 845.

(2) (a) Salem, A. K.; Searson, P. C.; Leong, K. W. *Nat. Mater.* **2003**, *2*, 668. (b) Heemeier, M.; Carlsson, A. F.; Naschitzki, M.; Schmal, M.; Bäumer, M.; Freund, H.-J. *Angew. Chem., Int. Ed.* **2002**, *41*, 4073. (c) Chen, M.; Chien, C.-L.; Searson, P. C. *Chem. Mater.* **2006**, *18*, 1595.

(3) Xie, R.; Kolb, U.; Li, J.; Basché, T.; Mews, A. *J. Am. Chem. Soc.* **2005**, *127*, 7480.

(4) (a) Alayoglu, S.; Nilekar, A. U.; Mavrikakis, M.; Eichhorn, B. *Nat. Mater.* **2008**, *7*, 333. (b) Yan, J.-M.; Zhang, X.-B.; Akita, T.; Haruta, M.; Xu, Q. *J. Am. Chem. Soc.* **2010**, *132*, 5326.

(5) (a) Lim, B.; Wang, J.; Camargo, P. H. C.; Jiang, M.; Kim, M. J.; Xia, Y. *Nano Lett.* **2008**, *8*, 2535. (b) Lee, Y. W.; Kim, M.; Kim, Z. H.; Han, S. W. *J. Am. Chem. Soc.* **2009**, *131*, 17036. (c) Tsuji, M.; Matsuo, R.; Jiang, P.; Miyamae, N.; Ueyama, D.; Nishio, M.; Hikino, S.; Kumagae, H.; Kamarudin, K. S. N.; Tang, X.-L. *Cryst. Growth Des.* **2008**, *8*, 2528.

(6) Asazawa, K.; Yamada, K.; Tanaka, H.; Oka, A.; Taniguchi, M.; Kobayashi, T. *Angew. Chem., Int. Ed.* **2007**, *46*, 8024.

(7) Blackman, J. A.; Evans, B. L.; Maaroof, A. I. *Phys. Rev. B* **1994**, *49*, 863.

(8) Berkowitz, A.; Mitchell, J. R.; Carey, M. J.; Young, A. P.; Zhang, S.; Spada, F. E.; Parker, F. T.; Hutton, A.; Thomas, G. *Phys. Rev. Lett.* **1992**, *68*, 3745.

(9) Barnas, J.; Fert, A. *Phys. Rev. Lett.* **1998**, *80*, 1058.

Published on Web 12/09/2010

by oxidation on the surface of zerovalent metal nanoparticles, and the magnetic interaction between metal (core) and metal oxide (shell) has been examined.[10] However, the preparation of metal−metal nanoparticles with core−shell structures remains a significant challenge, because the transition metals listed above have greater negative redox potential than do noble metals such as Au, Ag, and Pd. In the present, we focused on Ni−Co (core−shell) nanoparticles.

The Ni−Co system is particularly noted for complete liquid and solid solubility, because of the small lattice size mismatch between face-centered cubic (fcc) Ni and fcc Co (3.524 and 3.545 Å, respectively, according to JCPDS files 4-0850 (Ni) and 15-0806 (Co)). Ni−Co alloy nanoparticles were synthesized in both gas-phase and liquid-phase methods, as described below. To the best of our knowledge, there exists no report on the preparation of Ni−Co nanoparticles with core−shell structures.

Using gas−solid-phase methods, for example, the chemical vapor transport method,[11] homogeneous Ni−Co alloys were obtained, because of a rapid diffusion of Ni and Co atoms in the process under high temperatures above 900 K. Using liquid-phase methods at lower temperatures, such as microemulsion synthesis,[12] sol−gel methods,[13] various chemical reduction methods,[14] hydrothermal reactions,[15] and polyol methods,[16] relatively homogeneous Ni−Co alloys were obtained even at lower temperatures because both Ni^{2+} and Co^{2+} were simultaneously reduced by strong reducing agents such as hydrazine and $NaBH_4$. In the polyol method, using a weak reducing agent, the formation of Ni−Co alloy nanoparticles was identified by energy dispersive X-ray spectrometer (EDS) mapping of a single particle prepared by heating a mixture of nickel and cobalt acetate tetrahydrate in ethylene glycol solution at 413 K for 2 h.[17] Now, it would be highly desirable to construct a new synthesis method of Ni−Co nanoparticles with artificially designed structures, such as core−shell.

To obtain bimetallic core−shell nanoparticles in a high yield, each reduction of metal ions should progress separately in the reaction. The core−shell nanoparticles are formed through the reduction of metal (M_1) ion after the core nanoparticle (M_2) production and then the nucleation growth of M_1 as a shell on the surface of M_2. The heterogeneous nucleation of M_1 particles on the surface of M_2 nanoparticles occurs more easily than the homogeneous nucleation of the independent M_1 nanoparticles, because the free energy needed for the heterogeneous nucleation of the M_1 cluster on the M_2 surface (ΔG_s^*) is lower than that for the homogeneous nucleation of the sole M_1 nanoparticles (ΔG^*).[18]

The core−shell nanoparticles could be effectively formed using separate reduction reactions in two stages with different reaction temperatures through the above heterogeneous nucleation process. For example, Cu−Ni core−shell nanoparticles have been prepared using this technique.[19] Cu^{2+} or Ni^{2+} in formate complexes with oleylamine ligands were reduced at around 433 or 463 K, respectively, because of their widely differing redox potentials and reduction temperatures [$E^0(Ni^{2+}/Ni^0) = -0.257$ V, $E^0(Cu^{2+}/Cu^0) = 0.342$ V vs NHE]. In the mixture of Cu^{2+} and Ni^{2+} in formate complexes with oleylamine, Cu−Ni core−shell nanoparticles were formed through the reduction of Ni^{2+} at 463 K after the Cu core nanoparticle production at around 433 K. Furthermore, the technique of the use of Pt, Pd, and Ag core nanoparticles as seed nanocrystals and catalysts for the reduction of the metal ions forming a shell have been widely chosen to obtain core−shell nanoparticles in a high yield.[20] Miyake et al. pointed out that Pd nanoparticles catalyzed the reduction of Ni^{2+} with 1-propanol for Pd−Ni nanoparticle production.[20a] Tsuji et al. reported that Ag nanoparticles enhanced the reduction of Cu^{2+} to produce Ag−Cu core−shell nanoparticles in a high yield using the polyol method.[20b] The transition metal ions could be reduced on the surface of the noble (core) nanoparticles at lower temperatures than the reduction temperatures of the metal ions in the absence of Pt, Pd, and Ag.

The standard electrode potential of Co^{2+} is close to that of Ni^{2+} [$E^0(Co^{2+}/Co^0) = -0.280$ V vs NHE]. However, the reduction temperature of Co^{2+} in the complex is not the same as that of Ni^{2+}. Heating a cobalt(II) formate complex with oleylamine in solution resulted in CoO nanoparticles being readily formed by thermal decomposition of the complex at 463 K, at which temperature Ni^{2+} in the formate complex with oleylamine was reduced.[21] A higher reaction temperature is required for the reduction to Co^0. Therefore, we chose a technique similar to that of the use of the noble (core) nanoparticles to obtain Ni−Co core−shell nanoparticles, for the following reason. Ni metal is active for several catalytic reactions, such as hydrogenation[22] and cross-coupling,[23] although

(10) Wang, C.; Baer., D. R.; Amonette, J. E.; Engelhard, M. H.; Antony, J.; Qiang, Y. *J. Am. Chem. Soc.* **2009**, *131*, 8824.
(11) Bagkar, N.; Seo, K.; Yoon, H.; In, J.; Jo, Y.; Kim, B. *Chem. Mater.* **2010**, *22*, 1831.
(12) Ahmed, J.; Sharma, S.; Ramanujachary, K. V.; Lofland, S. E.; Ganguli, A. K. *J. Colloid Interface Sci.* **2009**, *336*, 814.
(13) Mattei, G.; De Julián Fernández, C.; Mazzoldi, P.; Sada, C. *Chem. Mater.* **2002**, *14*, 3440.
(14) Zhu, L.-P.; Xiao, H.-M.; Fu, S.-Y. *Eur. J. Inorg. Chem.* **2007**, 3947.
(15) Hu, M.-J.; Zhang, S.; Guo, S.-R.; Lin, B.; Zhang, M.; Yu, S.-H. *J. Am. Chem. Soc.* **2008**, *130*, 11606.
(16) Viau, G.; Fiévet-Vincent, F.; Fiévet, F. *Solid State Ionics* **1996**, *84*, 259.
(17) Jayakumar, O. D.; Salunke, H. G.; Tyagi, A. K. *Solid State Commun.* **2009**, *149*, 1769.
(18) In the case of the heterogeneous nucleation of the M_1 nanoparticles as a shell on the surface of the M_2 nanoparticles as a core, the free energy change (ΔG_s^*) needed for the heterogeneous nucleation of M_1 on the M_2 surface is given as follows:[18a] $\Delta G_s^* = \Delta G^* \{(2 + \cos\theta)(1 - \cos\theta)^2/4\}$ (ΔG^*: free energy needed for the homogeneous nucleation of M_1 in the absence of M_2. θ: contact angle of M_1 nucleus to the M_2 surface.) (a) Kashchiev, D. *Nucleation*; Butterworth Heinemann: Oxford, 2000.
(19) Yamauchi, T.; Tsukahara, Y.; Sakata, T.; Mori, H.; Yanagida, T.; Kawai, T.; Wada, Y. *Nanoscale* **2010**, *2*, 515.
(20) (a) Teranishi, T.; Miyake, M. *Chem. Mater.* **1999**, *11*, 3414. (b) Tsuji, M.; Hikino, S.; Tanabe, R.; Yamaguchi, D. *Chem. Lett.* **2010**, *39*, 334.
(21) (a) Sun, X.; Zhang, Y.-W.; Si, R.; Yan, C.-H. *Small* **2005**, *1*, 1081. (b) Mohamed, M. A.; Halawy, S. A.; Ebrahim, M. M. *J. Therm. Anal.* **1994**, *41*, 387. (c) Wanjun, T.; Donghua, C. *Chem. Pap.* **2007**, *61*, 329.

these activities were lower than those of Pt and Pd. Therefore, we have hypothesized that the low-temperature reduction of Co^{2+} could be achieved using Ni nanoparticles as a catalyst and, then, the nucleus of Co^0 could take place on the surface of Ni nanoparticles to form Ni−Co (core−shell) nanoparticles. Although no report has detailed the catalytic activity of Ni nanoparticles for the low-temperature reduction of Co^{2+} in a complex, in the present study, we have finally clarified the fact that Ni nanoparticles can act as a catalyst to reduce Co^{2+}.

A microwave-assisted chemical method was chosen for the present study. Under microwave irradiation, reactants are heated directly and quickly through the interaction of the oscillating electric and magnetic fields with the substances, and then, a reaction solution is heated uniformly in a vessel. Nucleus growth throughout the entire reaction vessel is, therefore, simultaneous and homogeneous, and particles with a narrow size distribution can be obtained within a short time.[24] To investigate different reduction processes of several metal ions, reproducible experiments with the same reaction conditions (the same reaction temperature with the same rate of temperature rise) are required. These temperature rises are easily controllable by self-regulated microwave power. Therefore, the microwave-assisted method is preferable to the conventional method for the preparation of monodispersed metal nanoparticles.

In the present study, we prepared structure-controlled Ni−Co (core−shell) nanoparticles by the reduction of Ni^{2+} and Co^{2+} in the corresponding formate or acetate complexes with oleylamine under microwave irradiation. The nanostructure of a single particle was precisely identified by X-ray diffraction (XRD) and EDS attached to the high-angle annular dark-field scanning transmission electron microscope (HAADF-STEM). In addition, the reduction mechanism of Co^{2+} on the surface of Ni nanoparticles was revealed from the experimental results. Ni−Co nanoparticles with different compositions and crystalline shapes could be prepared by changing the molar ratios of both Ni^{2+} and Co^{2+} and the nickel precursors used in the synthesis.

2. Experimental Section

2.1. Materials. Nickel(II) formate dihydrate (purity >95%), nickel(II) acetate tetrahydrate (>97%), and cobalt(II) formate dihydrate (>98.5%) were purchased from Kishida Chemical Co., Ltd. Oleylamine [= (*Z*)-9-octadecenylamine] (primary amine contents; >98.0%, oleylamine contents for total primary amine one; >70% (GC)) was purchased from Aldrich Co., Ltd. These reagents were used as supplied. Oleylamine reagent was used as ligands in nickel(II) or cobalt(II) complexes, as reducing agents for the metal ions, as surface modifying agents for the obtained nanoparticles, and as a solvent.

Table 1. Preparation of Ni, CoO, and Ni−Co Nanoparticles under MW Irradiation

entry	starting materials nickel/cobalt	ratio Ni/Co	temp[a]/K	time[b]/min
Ni-1	$(HCOO)_2Ni\cdot 2H_2O$ (**1a**)	1:0	463	30
Ni-2	$(CH_3COO)_2Ni\cdot 4H_2O$ (**1b**)	1:0	498	30
CoO-1	$(HCOO)_2Co\cdot 2H_2O$ (**2a**)	0:1	463	30
$Ni_{50}CO_{50}$	**1b**/**2a**	1:1	498	30
$Ni_{33}CO_{67}$		1:2	498	30
Formate-$Ni_{50}Co_{50}$	**1a**/**2a**	1:1	463	30
Ninano-$Ni_{50}Co_{50}$	Ni-1/**2a**	1:1	463	30

[a] Reaction temperature. [b] Hold time at reaction temperature.

2.2. Preparation of Co and Ni Precursors. The precursor, cobalt(II) formate complex with oleylamine ligands, was synthesized as described in our previous work.[25] The Co precursor was synthesized by stirring a mixture of cobalt(II) formate dihydrate (12.5 mmol) and oleylamine (125.0 mmol) at 393 K for 30 min. The reaction solution changed from a pink suspension to a purple homogeneous solution. The Ni precursor was prepared under the same reaction conditions, except for the use of nickel(II) acetate tetrahydrate (12.5 mmol) as a starting material. Caution: Note that the fat-soluble Ni complexes are referred to as carcinogens. It is preferable to wear suitable protective clothing, gloves, and eye/face protection during the experiment.

2.3. Preparation of Ni−Co Nanoparticles. Preparation conditions of Ni−Co nanoparticles are listed in Table 1.

2.3.1. $Ni_{50}Co_{50}$ and $Ni_{33}Co_{67}$ Nanoparticles. A schematic illustration of the experimental setup is represented in Figure S1 of the Supporting Information. Microwave heating was carried out by the use of a multimode 2.45 GHz microwave apparatus operated at 1.25 kW (Micro Denshi Co., Ltd.). The temperature of the reaction solution was measured using a fiber-optic thermometer (AMOTH TM-5886, Anritsu Meter Co., Ltd.), which was inserted directly into the solution. The Ni−Co nanoparticles with a molar ratio of [Ni]/[Co] = 1:1 were prepared as follows. The Ni and Co precursors were prepared from nickel acetate tetrahydrate or cobalt formate dihydrate (12.5 mmol) with oleylamine (125.0 mmol) as described above, respectively. These solutions were added together at room temperature. The molar ratio between Ni^{2+}, Co^{2+}, and oleylamine was 1:1:20. This solution was heated in a quartz cylindrical vessel of 100 mL at the rate of 10 K min^{-1} and then allowed to stand at 498 K for 30 min under bubbling nitrogen gas at a flow rate of 200 mL min^{-1}. The color of the solution changed to black at 498 K. The reaction solution was then cooled to room temperature within 5 min by soaking the vessel in an ice bath. The resultant particles were centrifuged, washed several times with methanol to remove residual organic components, and dried under vacuum at 343 K for 4 h. Black Ni−Co nanoparticles were obtained (denoted as $Ni_{50}Co_{50}$). The temperature profiles of the reaction plotted against time and microwave (MW) power are shown in Figure S2 of the Supporting Information. The yield of $Ni_{50}Co_{50}$ was 99.5 atom %, and the calculation procedure is described in detail in the Results section and in SI-2 (Supporting Information). Ni−Co nanoparticles prepared using other molar ratios,

(22) (a) Reshetenko, T. V.; Avdeeva, L. B.; Ismagilov, Z. R.; Chuvilin, A. L.; Ushakov, V. A. *Appl. Catal., A* **2003**, *247*, 51. (b) Asedegbega-Nieto, E.; Bachiller-Baeza, B.; Guerrero-Ruíz, A.; Rodriguez-Ramos, I. *Appl. Catal., A* **2006**, *300*, 120.
(23) (a) Tobisu, M.; Shimasaki, T.; Chatani, N. *Angew. Chem.* **2008**, *120*, 4944. (b) Lipshutz, B. H.; Tasler, S.; Chrisman, W.; Spliethoff, B.; Tesche, B. *J. Am. Chem. Soc.* **1999**, *121*, 5819.
(24) (a) Tsukahara, Y.; Nakamura, T.; Kobayashi, T.; Wada, Y. *Chem. Lett.* **2006**, *35*, 1396. (b) Tsukahara, Y.; Higashi, A.; Yamauchi, T.; Nakamura, T.; Yasuda, M.; Baba, A.; Wada, Y. *J. Phys. Chem. C* **2010**, *114*, 8965. (c) Mallikarjuna, N. N.; Varma, R. S. *Cryst. Growth Des.* **2008**, *8*, 291.
(25) Yamauchi, T.; Tsukahara, Y.; Sakamoto, T.; Kono, T.; Yasuda, M.; Baba, A.; Wada, Y. *Bull. Chem. Soc. Jpn.* **2009**, *82*, 1044.

[Ni]/[Co] = 1:2 (denoted as $Ni_{33}Co_{67}$), were obtained under the same reaction conditions.

2.3.2. Formate-$Ni_{50}Co_{50}$ and Ninano-$Ni_{50}C_{50}$. Other types of Ni−Co nanoparticles with molar ratios of [Ni]/[Co] = 1:1 were prepared using two different synthetic routes. First, $Ni_{50}Co_{50}$ nanoparticles (denoted as *Formate*-$Ni_{50}Co_{50}$) were prepared using nickel and cobalt formate dihydrate as starting materials. The Ni and Co precursors were prepared from either nickel formate dihydrate (12.5 mmol) or cobalt formate dihydrate (12.5 mmol) with oleylamine (125.0 mmol), respectively, as described above. These solutions were added together at room temperature. The solution was heated at the rate of 10 K min^{-1} and then allowed to stand at 463 K for 30 min under microwave irradiation. Black Ni−Co nanoparticles were obtained through the same washing process as that of $Ni_{50}Co_{50}$ nanoparticles.

Another $Ni_{50}Co_{50}$ nanoparticle sample (denoted as *Ninano*-$Ni_{50}C_{50}$) was prepared under the same reaction conditions as those for *Formate*-$Ni_{50}Co_{50}$ except for the following details. Ni nanoparticles, denoted as Ni-1 were prepared according to a procedure described in the following section. Co precursor was prepared from cobalt formate dihydrate (12.5 mmol) and oleylamine (125.0 mmol) as described above. Ni nanoparticles (Ni-1, 12.5 mmol), the Co precursor, and oleylamine (125.0 mmol) were added together. The molar ratio between Ni^0, Co^{2+}, and oleylamine was 1:1:20. The solution was heated at 463 K for 30 min under microwave irradiation. A *Ninano*-$Ni_{50}C_{50}$ sample was obtained.

2.4. Preparation of Ni Nanoparticles. The Ni precursor was synthesized by stirring a mixture of nickel formate dihydrate (25.0 mmol) and oleylamine (250.0 mmol) at 393 K for 30 min. This solution was heated at a rate of 10 K min^{-1} under microwave irradiation and allowed to stand at 463 K for 30 min under bubbling nitrogen gas. Black Ni nanoparticles were obtained through the same washing process as that of $Ni_{50}Co_{50}$ nanoparticles (denoted as Ni-1).

Another type of Ni nanoparticles (denoted as Ni-2) was prepared under the same reaction conditions as those for Ni-1 except for the following details. The Ni precursor was prepared under the same reaction conditions, except for the use of nickel(II) acetate tetrahydrate (25.0 mmol) as a starting material. The solution was heated at 498 K for 30 min under microwave irradiation.

2.5. Preparation of CoO Nanoparticles. The Co precursor was prepared under the same reaction conditions as those for Ni-1, except for the use of cobalt formate dihydrate (25.0 mmol). The purple homogeneous solution was heated under the same reaction conditions as for Ni-1 and then changed to a brown suspension. The Co^{2+} ion was not reduced to Co^0. Brown CoO nanoparticles (denoted as CoO-1) were obtained.

2.6. Instruments. The crystal phases of the powders were analyzed using a MultiFlex (Rigaku Co.) with a Cu Kα radiation source in the range of the 2θ Bragg angles = 20−120° at 40 kV and 40 mA. The size and morphology of the Ni−Co nanoparticles were characterized using a transmission electron microscope (TEM) operated at 200 kV with a Hitachi H-800 (Hitachi High-Technologies Co.). The solution was dropped onto a copper grid coated with a carbon film, and the grid was dried under vacuum. The concentrations of both Ni and Co atoms in the Ni−Co nanoparticles were characterized using a high-angle annular dark-field scanning transmission electron microscope (HAADF-STEM) operated at 200 kV with a Hitachi HD-2700. The distributions of Ni and Co atoms in a single particle were characterized by point analyses along the cross-section line on a single isolated particle using an EDAX-Genesis type energy dispersive X-ray spectrometer (EDS) attached to the HAADF-STEM, in which an electron beam with an accelerating voltage of 200 kV was focused to a spot on the specimen with a diameter of about 0.4 nm. The composition of the $Ni_{50}Co_{50}$ nanoparticle sample was determined using an inductively coupled plasma-atomic emission spectrometer (ICP-AES; Perkin-Elmer Optima 7300 DV). The sample was treated as follows. About 100 mg of the powder was dissolved in a mixture of concentrated HNO_3 (6 mL) and HCl (1 mL). The solution was diluted to about 1000 mg mL^{-1} for ICP determination. The amounts of surface modifying agent on the surface of the nanoparticles were determined by thermogravimetric analysis (TGA) using a Shimadzu TGA-50 analyzer. TGA was performed at a heating rate of 10 K min^{-1} in a nitrogen atmosphere at a flow rate of 100 mL min^{-1}. Magnetic susceptibility data were obtained in applied fields ranging between −30 and 30 kOe using a SQUID susceptometer (MPMS-5S, Quantum Design Co.). ^1H NMR spectra were recorded using a Joel jnm-GSX-400 (400 MHz). The measurement was taken in $CDCl_3$ using tetramethylsilane (TMS) as an internal standard.

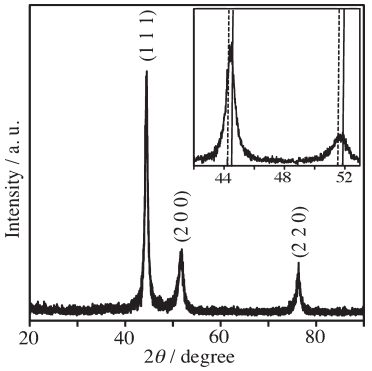

Figure 1. XRD pattern of $Ni_{50}Co_{50}$. The pattern enlarged in the 42−54° range is shown in the inset. The characteristic reflections corresponding to the (111) and (200) planes of bulk fcc Ni (solid line) and fcc Co (dotted line) are shown in the inset (JCPDS file 04-850 (Ni) and 15-0806 (Co)).

3. Results

3.1. Identification of the Structure of Ni−Co Nanoparticles. The crystal phase of the obtained powder was determined by powder X-ray diffraction (XRD) analysis. The XRD pattern of the $Ni_{50}Co_{50}$ nanoparticle sample is shown in Figure 1. The XRD reflection spectrum of $Ni_{50}Co_{50}$ was observed as an fcc pattern of (111), (200), and (311) planes. The two peaks of (111) and (200) planes were observed at 2θ = 44.4 and 51.7°, respectively. The 2θ angles of these planes of $Ni_{50}Co_{50}$ were larger than those of bulk fcc Co (44.2 and 51.5°) and smaller than those of bulk fcc Ni (44.5 and 51.8°), according to JCPDS files 4-0850 (Ni) and 15-0806 (Co), respectively. The obvious characteristic reflections corresponding to hexagonal (hcp) Co and fcc metal oxides (CoO and NiO) were not included in the spectrum of $Ni_{50}Co_{50}$. The XRD reflection spectrum of $Ni_{33}Co_{67}$ was the same fcc pattern as that of $Ni_{50}Co_{50}$.

The metal ratio ([Ni]/[Co]) in the $Ni_{50}Co_{50}$ nanoparticle sample was determined by ICP analysis. The weight proportions of Ni and Co were 47.6 and 47.3 wt %, respectively. The metal ratio ([Ni]/[Co] = 1.01) was coincident with the molar ratio [Ni^{2+}]/[Co^{2+}] used for the

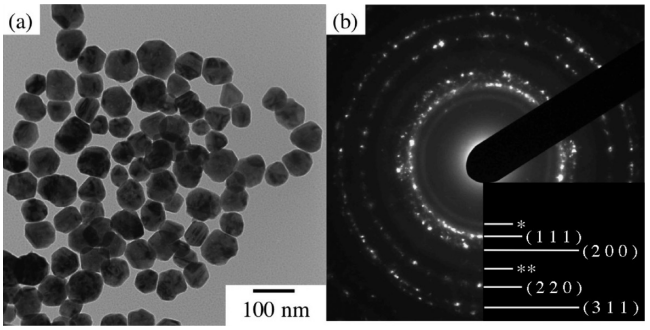

Figure 2. TEM image of $Ni_{50}Co_{50}$ and SAED pattern collected from the entire image in panel a (b). Debye rings of fcc metal were assigned as (hkl), and those of metal oxide were assigned as [*] (111) and [**] (220), respectively.

synthesis. The composition in the obtained powder was confirmed as $Ni_{50}Co_{50}$ from the ICP results. In order to determine organic component contents on the surface of the nanoparticles, TGA measurements were carried out. The weight-loss curve of the $Ni_{50}Co_{50}$ nanoparticles is shown in Figure S3 of the Supporting Information. The weight-loss percentage of the samples was 6.0 wt % at 723 K. The yield of the $Ni_{50}Co_{50}$ nanoparticle sample was calculated on the basis of the ICP and TGA results, as described in SI-2 (Supporting Information). The yield of $Ni_{50}Co_{50}$ was 99.5 atom %.

The TEM image and particle size distribution of the $Ni_{50}Co_{50}$ nanoparticle samples are shown in Figures 2a and S4 of the Supporting Information, respectively. The obtained nanoparticles were spherical in shape. The average particle size was 71.0 nm (standard deviation (σ): 13.7 nm), as determined from the TEM image of Figure 2a. The selected area electron diffraction (SAED) pattern obtained from the entire region in Figure 2a is shown in Figure 2b. The SAED pattern showed an fcc ring pattern of (111), (200), (220), and (311) planes. While the lattice spacing estimated from the pattern [(111) plane; 2.037 Å] was close to that of the fcc Ni or Co [(111) plane; 2.034 Å (Ni) or 2.046 Å (Co)], the value of the lattice spacing estimated by conventional TEM at 200 keV had a margin of error. It was, therefore, difficult to confirm whether the crystallite was a sole metal (Ni or Co) or a Ni−Co alloy. Another ring pattern, of the (111) (*) and (220) (**) planes, was blurred and is shown in Figure 2b. The lattice spacing estimated from this pattern was coincident with those of the fcc metal oxides (NiO or CoO). Identification of the metal oxide was difficult using the ring pattern of this blurry ring because both fcc NiO and CoO had a similar lattice spacing.[26] These results clearly indicated that Ni−Co nanoparticles containing a small amount of fcc NiO or fcc CoO were obtained.

The distributions of both Ni and Co atoms in one particle were characterized using HAADF-STEM. The HAADF-STEM image of $Ni_{50}Co_{50}$ is shown in Figure 3a.

(26) The lattice spacings of (111), (200), and (220) planes for fcc NiO and CoO according to JCPDS file 47-1049 (NiO) and 43-1004 (CoO) were the following: [(111); 2.412 Å (NiO) and 2.459 Å (CoO)], [(200); 2.089 Å (NiO) and 2.130 Å (CoO)], [(220); 1.476 Å (NiO) and 1.506 Å (CoO)].

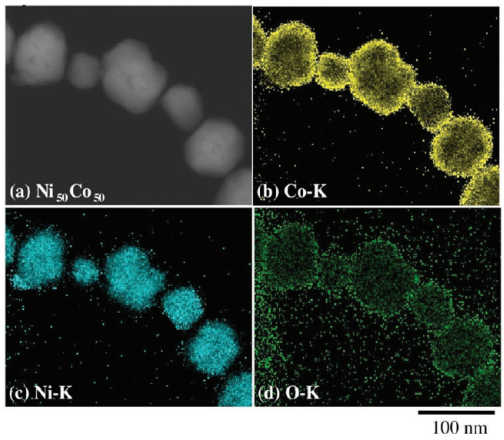

Figure 3. HAADF-STEM image of $Ni_{50}Co_{50}$ (a). Elemental maps of Co (b), Ni (c), and O (d) in the area shown in (a).

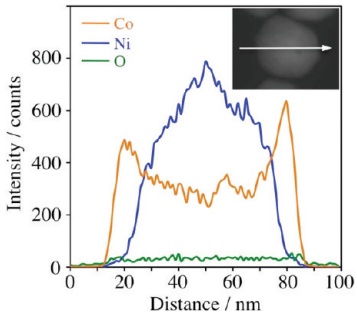

Figure 4. Cross-sectional compositional line profile on a single particle of $Ni_{50}Co_{50}$ indicated in the inset.

The particle sizes determined from the image agreed well with those from the TEM image in Figure 2a. Each elemental map of Ni, Co, and O in the area shown in Figure 3a was obtained using EDS attached to the HAADF-STEM shown in Figure 3b−d, respectively. Ni atoms were frequently seen in the center of the particles in the image. In contrast, the distribution of Co atoms became concentrated at the region close to the surface of the particles. In the outer layer of the particles, O atoms were found. The distributions of Ni, Co, and O atoms in a single particle are shown in Figure 4. The particles exposed to the electron beam for a long time would receive radiation damage. Therefore, a single particle shown in Figure 4 was used as a fresh single isolated particle in an area different from the measurement region shown in Figure 3a. The compositional line profile showed that Ni−Co nanoparticles ($Ni_{50}Co_{50}$) were composed of a Ni core with a diameter of ca. 46.9 nm surrounded by a Co shell, ca. 14.0 nm thick. These results indicated that Co shells were overgrown on Ni cores. However, the obtained nanoparticles were not simply separated as a pure Ni core and a pure Co shell region. In the region defined as the Co shell, the layer at a depth of ca. 10.0 nm from the outermost layer consisted chiefly of Co atoms. The layers in the proximity of depths of 10.0 and 14.0 nm from the outermost layer were composed of mixed Ni−Co alloy, in a region where the intensities of Co atoms were larger than those of Ni atoms. The nanostructure of $Ni_{50}Co_{50}$ was, therefore, identified as a Co-rich shell and a Ni-rich

Figure 5. Nanostructure of $Ni_{50}Co_{50}$ determined by HAADF-STEM.

core, as depicted in Figure 5. Furthermore, no independent Ni or Co nanoparticles were observed in 30 particles selected from other HAADF-STEM images. This result indicated that the Ni−Co (core−shell) nanoparticles could be produced in a high yield using our method. A HAADF-STEM image and elemental maps of $Ni_{33}Co_{67}$ are shown in Figure S5 of the Supporting Information. The nanostructure of $Ni_{33}Co_{67}$, with an average particle size of 57.0 nm (σ: 10.4 nm), was observed to be the same core−shell structure as that of $Ni_{50}Co_{50}$.

The distribution of O atoms in the $Ni_{50}Co_{50}$ sample, as shown in Figure 3d, became concentrated at a depth of ca. 2.0 nm from the surface of the particles. The result of the SAED pattern, as shown in Figure 2b, indicated that a small amount of fcc metal oxide (NiO or CoO) was contained in the $Ni_{50}Co_{50}$ nanoparticles. The combination of the HAADF-STEM and SAED results demonstrated that the nanostructure in one particle of $Ni_{50}Co_{50}$ consisted of a Co-rich shell and a Ni-rich core, with an interlayer of mixed Ni−Co alloy between the core and shell. Furthermore, the surface layer, at a depth of less than 2.0 nm from the outermost layer, was composed of fcc CoO. The Ni−Co nanoparticles prepared under bubbling nitrogen gas using this method could undergo oxidation when exposed to air at room temperature during the processes of washing and preparing the samples for measurements such as XRD and TEM. The XRD pattern of a $Ni_{50}Co_{50}$ sample stored for 4 months at room temperature under air atmosphere was unchanged from that of the same sample right after the isolation, as shown in Figure S6 of the Supporting Information. This result demonstrates that the initial oxidation on the surface of the Ni−Co (core−shell) nanoparticles is rapid, and then, the layer of the metal oxide (fcc CoO) forms. This is in agreement with the Cabrera−Mott theory on the oxidation of metals.[27] Cheng et al. reported that further growth of the fcc CoO shell was much slower after a rapid initial oxidation of Co nanocrystals.[28]

(27) (a) Motto, N. F. *Trans. Faraday Soc.* **1940**, *35*, 0472. (b) Chernavskii, P. A.; Pankina, G. V.; Chernavskii, A. P.; Peskov, N. V.; Afanasiev, P.; Perov, N. S.; Tennov, V. A. *J. Phys. Chem. C* **2007**, *111*, 5576.

(28) Cheng, G.; Dennis, C. L.; Shull, R. D.; Hight Walker, A. R. *Cryst. Growth Des.* **2009**, *9*, 3714.

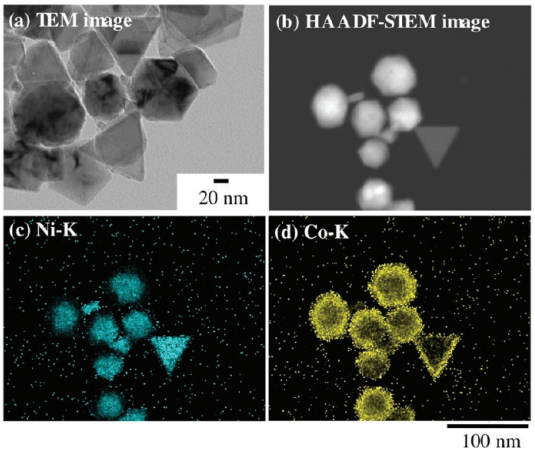

Figure 6. TEM (a) and HAADF-STEM (b) images of *Formate*-$Ni_{50}Co_{50}$. Elemental maps of Ni (c) and Co (d) in the area shown in (b).

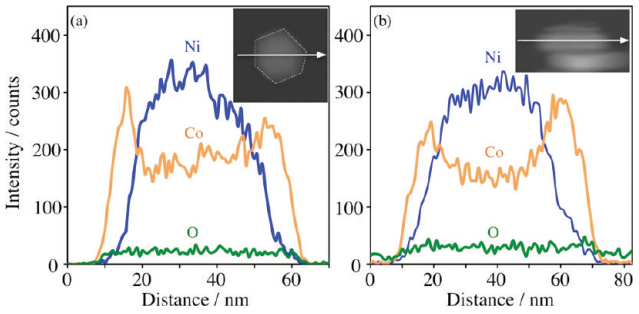

Figure 7. Cross-sectional compositional line profile on a single particle of *Formate*-$Ni_{50}Co_{50}$ indicated in the inset. Two line profiles were taken from the top (a) and side faces (b) of a hexagonal nanoplate.

In the synthesis of the sole Ni nanoparticles (Ni-1 or Ni-2) prepared from nickel formate or acetate salts, Ni-1 and Ni-2 were platelike and spherical nanoparticles, respectively. The TEM images of Ni-1 and Ni-2 are shown in Figures S7 and S8 of the Supporting Information. The crystalline shapes of Ni nanoparticles could be modified by changing the nickel precursors used in synthesis. On the basis of these results, another type of $Ni_{50}Co_{50}$ nanoparticle (*Formate*-$Ni_{50}Co_{50}$) was prepared from both nickel and cobalt formate dihydrate. The TEM and HAADF-STEM images of the *Formate*-$Ni_{50}Co_{50}$ nanoparticle sample are shown in Figure 6a,b, respectively. As seen in the TEM and HAADF-STEM images, the obtained nanoparticles were platelike in shape, such as triangular and hexagonal nanoplates like those of Ni-1. Each elemental map of Ni and Co in the area shown in Figure 6b is also shown in Figure 6c,d. A single triangular nanoplate in Figure 6b−d confirmed that Co atoms were deposited on the entire surface of the triangular Ni nanoplate. The line profiles taken from the top or side faces of a single hexagonal nanoplate are shown in Figure 7a,b. These profiles also indicated that Co atoms were deposited on the flat top and bottom faces, as well as the side faces of the Ni hexagonal nanoplate. These results demonstrated the successful preparation of a shape-controlled core−shell nanostructure consisting of the Ni nanoplate as a core and a complete shell of Co and indicated that the crystalline shapes of the Ni−Co

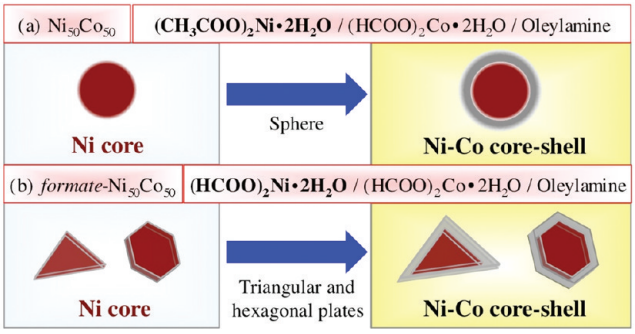

Figure 8. Schematic crystal structures of the Ni cores and Ni−Co (core−shell) nanocrystals prepared from nickel formate or acetate complexes with a cobalt formate complex.

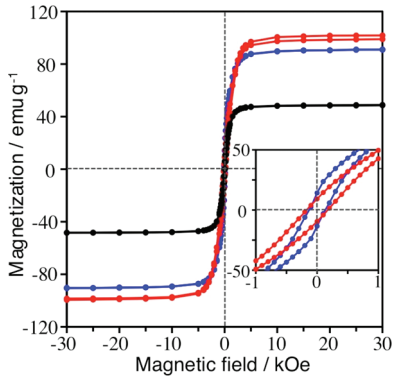

Figure 9. Magnetization versus applied field for $Ni_{50}Co_{50}$ (blue), $Ni_{33}Co_{67}$ (red), and Ni-2 (black) at 300 K. Inset shows a close-up of the region around zero.

(core−shell) nanoparticles depended on those of the Ni cores when Co shells were overgrown on Ni cores. The schematic crystal structures of various Ni−Co (core−shell) nanocrystals prepared from nickel formate or acetate complexes with a cobalt formate complex are shown in Figure 8. Ni-1, prepared from the nickel formate complex, was made up of triangular and hexagonal nanoplates. In a similar manner, *Formate*-$Ni_{50}Co_{50}$, prepared from the same complex with cobalt formate complex, was triangular and hexagonal. This result indicated that the Ni−Co (core−shell) nanoparticles were produced through the epitaxial growth of Co shells surrounding Ni cores. In the case of Ni-2 and $Ni_{50}Co_{50}$ using nickel acetate salt as a starting material, $Ni_{50}Co_{50}$ had the same spherical nanostructure as that of Ni-2. These results demonstrate that the crystallinity of the Ni core plays a key role in determining the final shape of a Ni−Co (core−shell) nanocrystal.

3.2. Magnetic Properties. The magnetic behavior of Ni−Co nanoparticles prepared by our method was examined using a SQUID susceptometer. Figure 9 shows a plot of magnetization versus applied fields at 300 K. The saturation magnetizations (σ_s) of Ni-2, $Ni_{50}Co_{50}$, $Ni_{33}Co_{67}$,

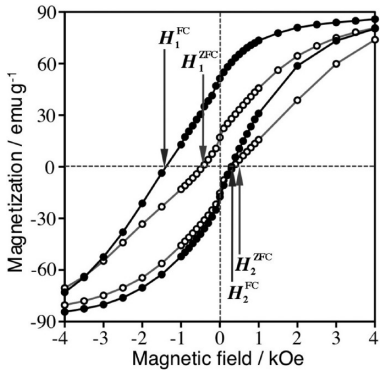

Figure 10. Hysteresis loops for $Ni_{50}Co_{50}$ after ZFC (●) and FC (○) at 10 K.

Table 2. Saturation Magnetization (σ_s), Coercivity (H_c), and Exchange Bias (H_{eb}) of $Ni_{50}Co_{50}$, $Ni_{33}Co_{67}$, Ni-2, and Co-1 at 10 K

	300 K	10 K		
sample	σ_s/emu g^{-1}	σ_s/emu g^{-1}	H_c/emu g^{-1}	H_{eb}/emu g^{-1}
Ni-2	48.6	50.8	201.6	10.3
$Ni_{50}Co_{50}$	90.7	91.2	396.4	545.7
$Ni_{33}Co_{67}$	99.7	102.3	573.2	561.7
Co-1	143.1	138.9	416.5	6.1

and carbon-coated Co nanopowders (denoted as Co-1)[29] at 300 K are listed in Table 2. The magnetic behavior of all samples was ferromagnetic. The values (σ_s) of $Ni_{50}Co_{50}$ and $Ni_{33}Co_{67}$ were 90.7 and 99.7 emu g^{-1} at 300 K, respectively, and larger than that of Ni-2 (48.6 emu g^{-1}), and these increased as the Co content increased (σ_s (bulk fcc Ni); 55.1 emu g^{-1} and σ_s (bulk hcp Co); 161.9 emu g^{-1} at 293 K).[30]

The effect of an oxide layer on the particle surface was examined for a hysteresis loop shift. Ferromagnetic (FM) Co or Ni nanoparticles coated with the corresponding antiferromagnetic (AFM) fcc metal oxide (CoO or NiO) have demonstrated exchange anisotoropy.[31] This phenomenon was explained by an exchange anisotropy interaction at the interface between the FM region of the metal particles and the surface layers of AFM metal oxide. Hysteresis loops versus applied fields were measured at 10 K after completion of both zero-field cooling (ZFC) and field cooling (FC) processes. In the FC process, the sample was cooled from 300 to 10 K in a magnetic field, H, of 1 T. Figure 10 shows the ZFC and FC loops obtained for $Ni_{50}Co_{50}$. At 10 K, an asymmetric magnetic hysteresis loop and a deviation between the ZFC and FC magnetization, which was commonly referred to as an exchange bias field (H_{eb}), were observed. The coercivity (H_c) and exchange bias (H_{eb}) of Ni−Co nanoparticles prepared using different molar ratios of Ni/Co are listed in Table 2. The H_{eb} ($=|H_1^{FC} + H_2^{FC}|/2$) of $Ni_{50}Co_{50}$ was calculated to be 545.7 Oe, which was indicative of an exchange bias effect. Under ZFC conditions, the

(29) Co-1 was purchased from Aldrich Co., Ltd., which was synthesized as described in the literature.[29a] The particle sizes were below 50 nm and Co-1 was covered by a carbon shell consisting of approximately three graphitic layers, which were identified from the TEM image shown in Figure S9 (Supporting Information). (a) Grass, R. N.; Athanassioy, E. K.; Stark, W. J. *Angew. Chem., Int. Ed.* **2007**, *46*, 4909.

(30) Lide, D. R. *CRC handbook of chemistry and physics*; CRC: Boca Raton, FL, 2008.

(31) (a) Nogués, J.; Sort, J.; Langlais, V.; Skumryev, V.; Suriñach, S.; Muñoz, J. S.; Baro, M. D. *Phys. Rep.* **2005**, *422*, 65. (b) Nogués, J.; Skumryev, V.; Sort, J.; Stoyanov, S.; Givord, D. *Phys. Rev. Lett.* **2006**, *97*, 157203. (c) Kimi, J. *J. Magn. Magn. Mater.* **2001**, *234*, 584. (d) Meiklejohn, W. H.; Bean, C. P. *Phys. Rev.* **1957**, *105*, 904.

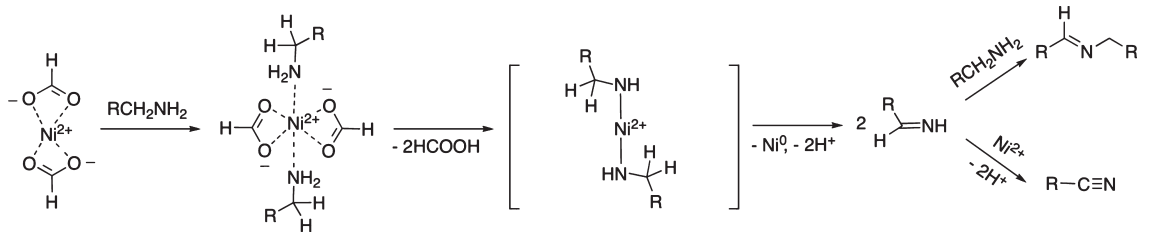

Figure 11. Schematic illustration of the proposed redox mechanism between nickel formate complex and primary amine.

H_c (= $|H_1^{ZFC} - H_2^{ZFC}|/2$) of $Ni_{50}Co_{50}$ was 396.4 Oe. When the samples of the obtained Ni−Co nanoparticles were cooled to below the Néel temperature of the AFM CoO (293 K)[30] in a magnetic field, exchange bias fields (H_{eb}) were observed as a result of exchange coupling at the AFM/FM CoO/Ni−Co interfaces. Above the Néel temperature, CoO was paramagnetic, and the exchange bias disappeared at 300 K, as shown in the inset of Figure 9. The magnetic properties of $Ni_{33}Co_{67}$, i.e., H_{eb} (561.7 Oe), were the same as those of $Ni_{50}Co_{50}$ at 10 K. However, Co-1 and Ni-2 showed a negligible H_{eb}, because Co-1 and Ni-2 were covered with a carbon shell or partially covered with NiO on the surface at a thickness of less than 0.5 nm, as characterized by X-ray photoelectron spectroscopy.[19]

4. Discussion

4.1. Mechanism of Ni−Co (Core−Shell) Nanoparticle Production. *4.1.1. Redox Mechanism between Ni^{2+} and Primary Amine*. Primary aliphatic amines have often been used as both a reducing agent for metal ions and a capping agent for the metal nanoparticles produced.[32] In the absence of primary amines, Ni^{2+} was reduced to Ni^0 through the thermal decomposition of nickel formate dihydrate at 503 K using tetraethylene glycol as a solvent.[25] In contrast, Ni^{2+} in the formate complex with the addition of primary amines was reduced at a lower temperature (463 K). These results indicated that this low-temperature reduction was due to the existence of primary amines, which acted as a reducing agent for Ni^{2+} in the formate complex at around 463 K.

A redox mechanism between metal ions and primary amine has been proposed by several reports on the reduction of Cu^{2+} and Ag^+.[33] Through the reduction of the metal ions (Cu^{2+} or Ag^+), the primary amines were converted to the corresponding imines, nitriles, and aldimines. On the basis of these results, we propose that Ni^{2+} in the formate complex with oleylamine could be reduced through the same reduction mechanism. A proposed redox mechanism between a nickel formate complex and a primary amine is shown in Figure 11. Initially, the mixture of a nickel(II) formate dihydrate and two primary amines forms a six-coordinated nickel complex composed of two bidentate formate ions and two monodentate amines.[25] The decomposition of the complex then takes place to form a nickel(II) amide species as an intermediate. A nickel amide then undergoes β-hydrogen elimination to produce a Ni^0 atom through an imine and a nickel hydride in an inert atmosphere.[34] In this process, the imines could be replaced with the corresponding nitriles by the dehydrogenation of the imines in the same manner as the oxidation of primary amines in the existence of Ni^{2+} with the aldimines by the addition of primary amines to the imines.

In order to confirm the proposed redox mechanism, it was absolutely imperative to examine the production of the imines, nitriles, and aldimines, along with the reduction of Ni^{2+}. Therefore, organic components in the reaction solution of Ni-1 were identified from the ^{1}H NMR spectra of the residual solution, from which the obtained nanoparticles were removed by centrifugation. The ^{1}H NMR spectrum of the Ni-1 solution is shown in Figure S10a of the Supporting Information. The ^{1}H NMR spectrum of the Ni-1 solution showed the existence of formamide, nitrile, and aldimine (See Supporting Information: SI-3 and Table S1). These results indicated that the existence of nitrile and aldimine in the three components supported the proposed redox mechanism. Oleylamine could act as a reducing agent for Ni^{2+} at 463 K. The nitrile and aldimine were produced along with the oxidation of oleylamine. Formamide was produced through the Ni nanoparticle production. It was speculated that formamide was not produced along with the oxidation of oleylamine in the proposed redox mechanism but was produced by the condensation of oleylamine with the formate ion that was dissociated from the nickel(II) formate complex along with the formation of Ni nanoparticles.

4.1.2. Redox Mechanism between Co^{2+} and Primary Amine in the Presence of Ni Nanoparticles. Co^{2+} in a formate complex with oleylamine could not be reduced to Co^0 but converted to CoO nanoparticles at 463 K, denoted as CoO-1. The TEM image, particle size distribution, and XRD pattern of CoO-1 are shown in Figures S11 and S12 of the Supporting Information, respectively. The average particle size of CoO-1 was 28.0 nm (σ: 3.5 nm). To obtain Co nanoparticles, heating under high temperatures above 553 K was required.[35]

In the presence of the prepared Ni nanoparticles (Ni-1), Co^{2+} in a formate complex with oleylamine was reduced

(32) (a) Hiramatsu, H.; Osterloh, F. E. *Chem. Mater.* **2004**, *16*, 2509. (b) Carenco, S.; Boissiére, C.; Nicole, L.; Sanchez, C.; Le Floch, P.; Mézailles, N. *Chem. Mater.* **2010**, *22*, 1340.
(33) (a) Capdevielle, D.; Lavigne, A.; Sparfel, D.; Baranne-Lafont, J.; Cuong, N. K.; Maumy, M. *Tetrahedron Lett.* **1990**, *31*, 3305. (b) Chen, M.; Feng, Y.-G.; Wang, X.; Li, T.-C.; Zhang, J.-Y.; Qian, D.-J. *Langmuir* **2007**, *23*, 5296.
(34) Yamaguchi, K.; Mizuno, N. *Angew. Chem., Int. Ed.* **2003**, *42*, 1480.
(35) Co nanoparticles were prepared under the same reaction conditions as those for CoO-1 except for the reaction temperature (553 K). The XRD spectra and TEM image of the obtained Co nanoparticles are shown in Figure S13 (Supporting Information).

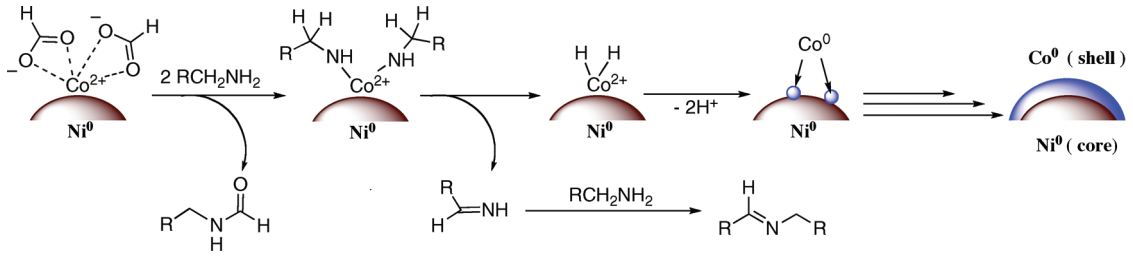

Figure 12. Schematic illustration of a proposed mechanism for the formation of Ni−Co (core−shell) nanoparticles.

at 463 K to produce Ni−Co nanoparticles, denoted as *Ninano*-$Ni_{50}Co_{50}$. The XRD spectrum of *Ninano*-$Ni_{50}Co_{50}$, as shown in Figure S14 of the Supporting Information, was observed to be the same fcc pattern as that of $Ni_{50}Co_{50}$. Therefore, we hypothesized that Co^{2+} was reduced on the surface of Ni nanoparticles at a temperature that was lower than that for the sole Co nanoparticles in the absence of Ni nanoparticles. Ni nanoparticles could act as a catalyst for the redox reaction between Co^{2+} and oleylamine. To clarify the catalytic activity of Ni nanoparticles for the low-temperature reduction of Co^{2+} in the complex, three kinds of organic components (formamide, nitrile and aldimine) in the reaction solution of CoO-1 and *Ninano*-$Ni_{50}Co_{50}$ were identified from the ^{1}H NMR spectra. The ^{1}H NMR spectra of the CoO-1 and *Ninano*-$Ni_{50}Co_{50}$ solutions are shown in Figures S15 and S16 of the Supporting Information, respectively. The content ratios for the three components listed above and oleylamine in the reaction solutions of CoO-1 and *Ninano*-$Ni_{50}Co_{50}$ are shown in Table S1 of the Supporting Information. The ^{1}H NMR spectrum of the CoO-1 solution showed the existence only of formamide and oleylamine. On the other hand, the ^{1}H NMR spectrum of the *Ninano*-$Ni_{50}Co_{50}$ solution showed the existence of all three components, as in that of Ni-1. This result demonstrated that Ni nanoparticles could act as a catalyst for the redox reaction between Co^{2+} and oleylamine and lower the reduction temperature of Co^{2+}. In contrast, a sole Co^{2+} in a formate complex with oleylamine was converted to CoO nanoparticles through the decomposition of the complex.[36]

4.1.3. Formation Mechanism of Ni−Co (Core−Shell) Nanoparticles in a One-Pot Reaction. The sole Ni nanoparticles (Ni-2), prepared from nickel acetate salt and oleylamine, were obtained at 498 K. In the one-pot reaction of $Ni_{50}Co_{50}$ (core−shell) nanoparticles, $Ni_{50}Co_{50}$ nanoparticles were obtained under the same reaction conditions as that of Ni-2 except for the concentration of Ni^{2+}. The molar ratio of $[Ni^{2+}]$/[oleylamine] used for Ni-2 was the same as that of $([Ni^{2+}]+[Co^{2+}])$/[oleylamine] for $Ni_{50}Co_{50}$. The diameter of a Ni core in a $Ni_{50}Co_{50}$ nanoparticle was ca. 46.9 nm and approximately half that of Ni-2 (98.5 nm).

From these results, we propose the formation mechanism of Ni−Co (core−shell) nanoparticles through the following heterogeneous nucleation process. A proposed mechanism is shown in Figure 12. Initially, Ni nanoparticles are produced at around 498 K according to the redox mechanism shown in Figure 11, and then, the Ni nanoparticles grow to a size of ca. 45 nm. Next, Co^{2+} is reduced on the surface of the Ni nanoparticles, and then, a nucleus of Co^0 is generated. Finally, Co shells are overgrown on the Ni core, and Ni−Co (core−shell) nanoparticles are produced.

4.1.4. Role of Microwave Irradiation in Ni−Co (Core−Shell) Nanoparticle Production. To investigate the microwave effect on the core−shell formation of Ni−Co nanoparticles, Ni−Co (core−shell) nanoparticles were prepared using an oil bath under the same reaction conditions as that of *Ninano*-$Ni_{50}Co_{50}$. The heterogeneous solution containing Ni nanoparticles and soluble cobalt formate complex with oleylamine was heated at 463 K for 30 min in an oil bath. The reaction solution immediately changed from a purple heterogeneous solution to a black suspension. This result indicated that Co^{2+} could be easily reduced to Co^0 in the presence of Ni nanoparticles even in the conventional method. Therefore, we speculate that Ni−Co nanoparticles with core−shell structures could be prepared even in the conventional method by considering the reaction conditions on the basis of our proposed formation mechanism of Ni−Co (core−shell) nanoparticles.

Under microwave irradiation, a reaction solution is heated uniformly and quickly in a vessel. Therefore, nucleus growth throughout the entire reaction vessel is simultaneous and homogeneous, and metal nanoparticles with a narrow size distribution can be obtained within a short time.[24] We have reported on the preparation of Ni nanoparticles with a narrow size distribution synthesized under very similar reaction conditions in our previous paper.[24b] The difference between the microwave-assisted method and the conventional method was examined in the synthesis of Ni nanoparticles using nickel formate dihydrate with oleylamine. In the microwave-assisted method, Ni nanoparticles with a narrow size distribution could be easily obtained rather than those obtained in the conventional method. In a similar manner, Ni−Co (core−shell) nanoparticles with a narrow size distribution could be easily obtained because of the uniform and rapid heating under microwave irradiation.

4.1.5. Differences in the Formation Mechanisms of Bimetallic Core−Shell Nanoparticles. We have reported on the rapid preparation of Cu−Ni (core−shell) nanoparticles

(36) (a) Khimchenko, Y. I.; Vasilenko, V. P.; Radkevich, L. S.; Myalkovskii, V. V.; Chubar, T. V.; Chegoryan, V. M. *Powder Metall. Met. Ceram.* **1977**, *16*, 327. (b) Wang, X.; Lu, L.; Wu, P.; Song, Q.; Wang, X. *Thermochim. Acta* **1990**, *165*, 139.

using formate complexes of Cu^{2+} and Ni^{2+} with oleylamine under microwave irradiation.[19] The synthesis technique of Ni−Co (core−shell) nanoparticles is similar to that of Cu−Ni (core−shell) nanoparticles based on the two perspectives, using the similar precursors except for the metal ions and a one-pot reaction under microwave irradiation. However, the reduction mechanisms of the metal ions forming a shell are different between Cu−Ni and Ni−Co (core−shell) nanoparticles. In the case of Ni−Co (core−shell) nanoparticle production, Co^{2+} on the surface of the Ni nanoparticles is reduced at a temperature that is lower than that of a sole Co^{2+} in a formate complex with oleylamine, and then, Co shells are overgrown on the Ni core. Ni core nanoparticles can act as a catalyst for the redox reaction between Co^{2+} and oleylamine, while Cu−Ni (core−shell) nanoparticles are formed through the reduction of Ni^{2+} at 463 K after Cu core nanoparticle production at around 433 K. The reduction temperature of Ni^{2+} is in accordance with that of a sole Ni^{2+} in a formate complex with oleylamine. This result indicates that Cu core nanoparticles cannot act as a catalyst. Therefore, Cu−Ni (core−shell) nanoparticles must be formed using a separate reduction reaction in two stages with different reaction temperatures.

5. Conclusions

In summary, we were successful in the rapid preparation of Ni−Co (core−shell) nanoparticles in a one-pot reaction under microwave irradiation. Observation using the HAADF-STEM technique showed the nanostructure was composed of a Co-rich shell and a Ni-rich core. A formation mechanism for Ni−Co nanoparticles was proposed and was based on the results of several synthetic routes. Ni nanoparticles catalyzed the reduction of Co^{2+} with oleylamine. Co^{2+} was reduced on the surface of the Ni nanoparticles, and then, Co shells were overgrown on the Ni core to form Ni−Co (core−shell) nanoparticles. The composition and crystalline shapes of the Ni−Co nanoparticles were easily controlled by changing the molar ratios of Ni/Co and different nickel precursors used for synthesis, respectively. The crystalline shapes depended on those of the Ni core of the nanoparticles. It is expected that these Ni−Co nanoparticles, combining properties of both Ni and Co, may be useful in many applications including catalytic oxidation, hydrogenation, and hydrogen storage.

Acknowledgment. This work was financially supported by the Nippon Steel Chemical Co., Ltd., Japan, by the Iwatani International Co., Ltd., Japan, and by Grant-in-Aid for Scientific Research on Priority Areas (No. 1807006, "Science and Technology of Microwave-Induced Thermally Non-Equilibrium Reaction Fields") from Ministry of Education, Culture, Sports, Science, and Technology, Japan.

Supporting Information Available: Experimental details (SI-1−SI-4) and Figures S1−S17 (PDF): Schematic view of the experimental setup and time profile of temperature under microwave irradiation during the synthesis of $Ni_{50}Co_{50}$, XRD patterns of *Ninano*-$Ni_{50}Co_{50}$, CoO-1 and Co nanoparticles, TEM images of Ni-1, Ni-2, Co-1 and CoO-1, HAASF-STEM image of $Ni_{33}Co_{67}$, TGA measurements of Ni−Co (core−shell) nanoparticles, ^1H NMR spectra of the Ni-1, CoO-1 and *Ninano*-$Ni_{50}Co_{50}$ solutions, and description about the content ratios of formamide, nitrile and aldimine in the above solutions This material is available free of charge via the Internet at http://pubs.acs.org.